Investigation of Sensitizer Adsorption and the Influence of Protons on Current and Voltage of a Dye-Sensitized Nanocrystalline TiO_2 Solar Cell

Md. K. Nazeeruddin,*,† R. Humphry-Baker, P. Liska, and M. Grätzel*

Laboratory for Photonics and Interfaces, Institute of Molecular and Biological Chemistry, School of basic Sciences, Swiss Federal Institute of Technology, CH-1015 Lausanne, Switzerland

Received: December 31, 2002; In Final Form: March 10, 2003

FTIR spectra of $[Ru(dcbpyH_2)_2(NCS)_2]$ (N3), $(Bu_4N)_2[Ru(dcbpyH)_2(NCS)_2]$ (N719), and $(Bu_4N)_4[Ru(dcbpy)_2(NCS)_2]$ (N712) complexes measured as solid samples in photoacoustic mode display fine resolution of IR bands and exhibit differences between the cis and the trans carboxylic acid groups. The interaction between N3, N719, and N712 sensitizers with nanocrystalline TiO_2 film was investigated by ATR-FTIR spectroscopy. The data show that these complexes are being anchored onto the TiO_2 surface in bridging coordination mode using two out of their four carboxylic acid groups, which are trans to the NCS ligand. The effect of protons on both the short circuit photocurrent and the open circuit photovoltage of dye-sensitized nanocrystalline solar cells was scrutinized. For the standard electrolyte formulation employed and $TiCl_4$ treated mesoporous TiO_2 films, the monoprotonated form of the N3 dye exhibited superior power conversion efficiency under AM 1.5 sun compared to the four, two, and zero proton sensitizers.

1. Introduction

Dye-sensitized solar cells are currently attracting widespread academic and commercial interest for the conversion of sunlight into electricity because of its low cost and high efficiency.[1−19] In these cells, undoubtedly, the dyes and the mesoporous titania films are two of the key components for high-power conversion efficiencies. Several ruthenium complexes containing anchoring groups such as carboxylic acid, dihydroxy, and phosphonic acid on pyridine ligands have been used as dyes.[20−22] The anchoring groups serve to immobilize the dye on the nanocrystalline TiO_2 surface. The immobilized sensitizer absorbs a photon (eq I) to produce an excited state (eq II), which transfers efficiently its electron onto the TiO_2 conduction band. The oxidized dye is subsequently reduced by electron donation from an electrolyte containing the iodide/triiodide redox system (eq III). The injected electron flows through the semiconductor network to arrive at the back contact and then through the external load to the counter electrode (platinum sputtered conducting glass). At the counter electrode, reduction of triiodide in turn regenerates iodide (eq IV), which completes the circuit. To achieve high quantum yields of the excited state electron transfer process, the dye ideally needs to be in intimate contact with the semiconductor surface.

$$S(\text{adsorbed on } TiO_2) + h\upsilon \rightarrow S^*(\text{adsorbed on } TiO_2) \quad \text{(I)}$$

$$S^*(\text{adsorbed on } TiO_2) \rightarrow S^+(\text{adsorbed on } TiO_2) + e^-(\text{injected}) \quad \text{(II)}$$

$$S^+(\text{adsorbed on } TiO_2) + {}^3/_2I^- \rightarrow S(\text{adsorbed on } TiO_2) + {}^1/_2I_3^- \quad \text{(III)}$$

$$I_3^-(\text{cathode}) + 2e^- \rightarrow 3I^-(\text{cathode}) \quad \text{(IV)}$$

The anchoring groups of the sensitizer that contain protons, upon adsorption transfers most of its protons to the TiO_2 surface, charging it positively, and thereby the Fermi level moves down (positively).[23] The electric field associated with the surface dipole generated in this fashion enhances the adsorption of the ruthenium complex and assists electron injection from the excited state of the sensitizer into the titania conduction band, favoring higher photocurrents. However, the positive shift of the Fermi level decreases the gap between the redox couple iodide/triiodide and the Fermi level, resulting in lower open-circuit potential (Figure 1). On the other hand, if the sensitizer carries zero protons, then the Fermi level moves negatively due to adsorption of anionic complex and the cations thereby a higher value for open-circuit potential whereas that of short circuit current is low.[24−26] Therefore, there should be an optimal degree of protonation of the sensitizer for which the product of short circuit photocurrent and open circuit potential is high that determines the power conversion efficiency of the cell. The overall conversion efficiency (η) of the dye-sensitized solar cell is determined by the photocurrent density (i_{ph}), the open circuit potential (V_{oc}), the fill factor (ff) of the cell, and the intensity of the incident light (I_s), as shown in eq V. In this paper, we report the mode of adsorption of *cis*-dithiocyanatobis(2,2′-bipyridine-4,4′-dicarboxylate)ruthenium(II) sensitizer (N3) on TiO_2 and the influence of protons on the current and the voltage of the dye-sensitized solar cell.

$$\eta_{\text{global}} = i_{ph}V_{oc}\text{ff}/I_s \quad \text{(V)}$$

2. Experimental Section

2.1. Materials. All the solvents and the chemicals (puriss grade) were obtained from Fluka. The ruthenium complexes $[Ru(dcbpyH_2)_2(NCS)_2]$ (N3), $(Bu_4N)_4[Ru(dcbpy)_2(NCS)_2]$ (N712), and $(Bu_4N)_2[Ru(dcbpyH)_2(NCS)_2]$ (N719) were available from our previous studies.[27] The monoprotonated dye was prepared

† E-mail: MdKhaja.Nazeeruddin@epfl.ch.

10.1021/jp022656f CCC: $25.00
Published on Web 07/23/2003

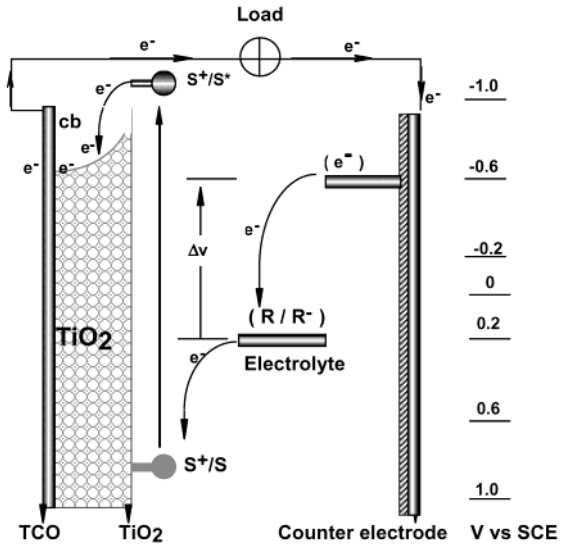

Figure 1. Operating principles and energy level diagram of dye-sensitized solar cell. $S/S^+/S^*$ = sensitizer in the ground, oxidized, and excited state, respectively. R/R^- = redox mediator (I^-/I_3^-).

using the following procedure. A 30 mg sample of the N719 dye was dispersed in 5 mL of water in a 20 mL flask. To this solution was added slowly tetrabutylammonium hydroxide solution with stirring (16 mg of 40% tetrabutylammonium hydroxide solution in water, which was further diluted in 2 mL of water). After dissolving the solid completely, the solution was evaporated. The resulting solid was recrystallized from ethanol and diethyl ether. The TiO_2 electrodes were prepared as described in the literature.[28]

2.2. Analytical Measurements. The FTIR spectra for all the samples were measured using a Digilab 7000 FTIR spectrometer. The ATR data reported here were taken with the "Golden Gate" diamond anvil ATR accessory (Graseby-Specac) using typically 64 scans at a resolution of 2 cm^{-1}. The samples were all measured under the same mechanical force pushing the samples in contact with the diamond window. No ATR correction has been applied to the data. It also has to be appreciated that this ATR technique probes at most 1 μm of sample depth and that this depends on the sample refractive index, porosity etc. Some of the spectra show artifacts due to attenuation of light by the diamond window in the 2000−2350 cm^{-1} region of the spectrum. The photoacoustic spectra (PAS) were measured with a MTEC 300 photoacoustic accessory that plugged directly into the same spectrometer. Samples were measured under He gas. The IR optical bench was flushed with dry air. The dye-coated TiO_2 films were rinsed in acetonitrile and dried at 150°C before taking the spectra. The FTIR spectra of anchored dyes were obtained by subtracting the IR spectrum of the blank TiO_2 films from the IR spectrum of the dye coated TiO_2 films of the same thickness. For comparison of various peak intensities the bipyridine ring mode intensity at 1544 cm^{-1} was used as an internal standard.

Proton and ^{13}C NMR spectra were measured on a Bruker 200 MHz spectrometer in CD_3OD. The reported chemical shifts were against TMS. UV−vis and fluorescence spectra were recorded in a 1 cm path length quartz cell on a Cary 5 spectrophotometer and Spex Fluorolog 112 spectrofluorometer, respectively.

2.3. Photovoltaic Measurements. Photoelectrochemical data were measured using a 450 W xenon light source that was focused to give 1000 W/m^2, the equivalent of 1 sun at AM1.5, at the surface of the test cell. The 12 μm thick TiO_2 electrodes were heated at 450 °C for 20 min under an O_2 atm and allowed to cool to 100 °C before dipping them into the dye solution. The N3 and N719 dye solutions were prepared in 1:1 acetonitrile and *tert*-butyl alcohol solvents. The typical concentrations were in the range of 5×10^{-4} M and the electrodes were left in the dye solutions for 12−15 h. The monoprotonated dye solution was prepared in 5% ethanol and 95% *tert*-butyl alcohol of concentration 3×10^{-4}, and the electrodes were left in the solution for 24 h. The N712 solutions were prepared in acetonitrile, concentration of 2×10^{-2} M. The concentrated solutions were dropped onto the surface of TiO_2 electrode and left the dye solution for 5 min. Then the electrodes were rinsed with acetonitrile and the dye deposited film is used as such in photovoltaic measurements.

A sandwich cell was prepared by using the dye anchored TiO_2 film as a working electrode and a second conducting glass coated with chemically deposited platinum from 0.05 M hexachloroplatinic acid as a counter electrode. The two electrodes were superimposed with a thin transparent film of Surlyn polymer gasket (DuPont). The superimposed electrodes were tightly held and applied heat (130°C) around the Surlyn gasket to seal the two electrodes. A thin layer of electrolyte containing 0.6 mol of (dimethylpropyl)imidazolium iodide, and 50 mmol of I_2, in methoxyacetonitrile was introduced into the interelectrode space from the counter electrode side through a predrilled hole. Then, the drilled hole was sealed with a microscope cover slide and Surlyn to avoid leakage of the electrolyte solution.

3. Results and Discussion

3.1. Photoacoustic FTIR Spectra of $[Ru(dcbpyH_2)_2(NCS)_2]$ (N3), $(Bu_4N)_4[Ru(dcbpy)_2(NCS)_2]$ (N719), and $(Bu_4N)_4[Ru(dcbpy)_2(NCS)_2]$ (N712). The molecular structures of the N3, N719, and N712 complexes are shown in Chart 1. They differ in the number of protons four, two, and zero, respectively. A comparison of FTIR spectra obtained in PAS mode using solid samples of N3, N719, and N712 are shown in Figure 2. The FTIR spectra of the N3 complex (Figure 2a) show the characteristic band at 2123 cm^{-1} due to the υ(NCS) group. The two distinct bands at 1740 and 1708 cm^{-1} are assigned tentatively to the C═O stretching of the cis carboxylic groups (carboxylic groups trans to the NCS ligands) and the trans carboxylic groups (carboxylic groups trans to pyridine). The apparent difference between cis and trans carboxylic acid groups in the N3 complex is consistent with its ground-state pK_a's, which are found to occur in two steps at 3 (pK_{a1}) and 1.5 (pK_{a2}).[27] These values are assigned to concurrent dissociation of two protons coming from the cis and trans carboxylic acid groups, respectively. The IR data are also in agreement with ^{13}C NMR spectra discussed in the NMR section. The FTIR, the pK_a, and the ^{13}C NMR data unambiguously show that the difference in the cis and the trans carboxylic acid groups of the N3 complex is measurable by various spectroscopic techniques. The two peaks at 1273 and 1242 cm^{-1} are assigned to the υ(C−O) stretch. The sharp and slightly weaker bands at 1617, 1551, and 1421 cm^{-1} are assigned to the bipyridyl υ(C═C) absorption.

The photoacoustic FTIR spectra of the N719 complex (Figure 2b) show the presence of carboxylic acid and the carboxylate groups. The bands at 1719 and 1235 cm^{-1} are assigned to the υ(C═O) and υ(C−O) groups, respectively. The other two strong bands at 1627 ($-COO^-_{as}$) and 1375 ($-COO^-_{s}$) cm^{-1} are assigned to the asymmetric and the symmetric stretch of the carboxylate group, respectively. The bands at 1627, 1543, and 1409 cm^{-1} are assigned to the bipyridyl absorption. The band

CHART 1

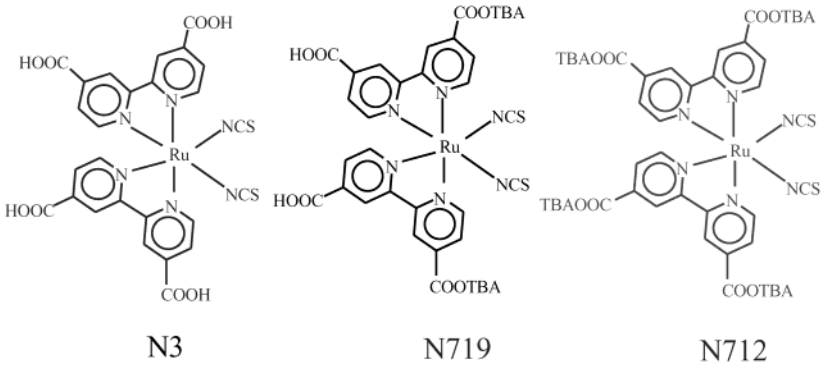

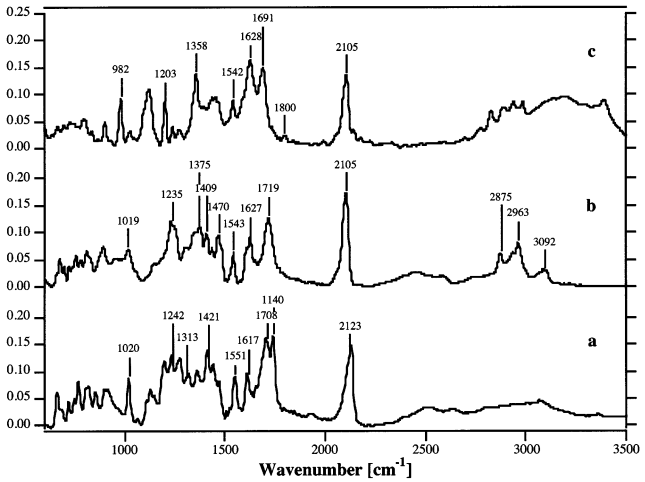

Figure 2. FTIR spectra of N3 (a), N719 (b), and N712 (c) obtained in photoacoustic mode using solid samples.

at 1470 cm^{-1} is assigned to the $\delta(CH_2)$ of the Bu_4N^+ cations.[29] The FTIR spectra of the N712 complex (Figure 2c) show the presence of carboxylate groups at 1690 and 1627 due to the asymmetric stretch of the cis and the trans carboxlate groups ($-COO^-_{as}$). The corresponding symmetric stretch ($-COO^-_s$) was observed at 1358 cm^{-1}. The bands at 2858, 2931, 2873, and 2960 cm^{-1} in N719 and N712 are assigned to υ(C−H) of tetrabutylammonium symmetric and asymmetric $-CH_2$ and $-CH_3$ groups, respectively.[29] The υ(NC) band in N719 and N712 was observed at 2105 cm^{-1}, which is shifted to lower energy compared to the NCS band in the N3 complex (2123 cm^{-1}).

3.2. Surface Chelation of Polypyridyl Complexes onto the TiO_2 Oxide Surface. The carboxylate functional groups of the dye serve as grafting agents for the oxide surface of the TiO_2 films. The grafting of polypyridyl complexes onto the oxide surface, which allows for electronic communication between the complex and the substrate, is an important feature in a dye-sensitized solar cell. To achieve high quantum yields of the excited state electron transfer process, the dye ideally needs to be in intimate contact with the semiconductor surface. The ruthenium complexes that have carboxylic acid and phosphonic acid groups show electron-transfer yields in the range 80−100%. The near quantitative electron injection efficiency indicates a close overlap of the ligand π^* orbitals and the titanium 3d orbitals.

Several groups have focused their attention on fundamental aspects of dye-sensitized solar cell components. The interaction of the sensitizer with nanocrystalline TiO_2 films,[30,31] dynamics of electron injection processes on the semiconductor,[32,33] photophysical and electrochemical properties of the sensitizer have been investigated.[34,35] Despite all of these studies, the anchoring nature of the sensitizer on the semiconductor surface has not been fully revealed. Yanagida et al. concluded that the *cis*-dithiocyanatobis(2,2′-bipyridine-4,4′-dicarboxylate)ruthenium-(II) sensitizer (N3) sensitizer binds to the surface using ester-like and chelating linkages.[36] Woolfrey et al. have reported that the N3 complex anchors on the surface of TiO_2 in a bidentate or bridging mode.[29] However, Fillinger and Parkinson studied the adsorption behavior of the N3 sensitizer and found that the initial binding involves one carboxylate, with subsequent binding of two or more carboxylate groups on the surface.[30]

On the basis of the crystal structure of the N3 dye, Shklover et al. have postulated upon the possible anchoring modes of the sensitizer on the TiO_2.[31] In their modeling, the initial attachment of the dye is a single bond A-type (Figure 3). The main feature of this type of anchoring is the great rotational freedom of the molecule, which leads to immediate capture of carboxylic group by a neighboring Ti atom, resulting in anchoring B- and C-types. When the sensitizer N3 anchors on to TiO_2 surface using both carboxylic groups of the same bipyridyl ligand, this results in a two-bond anchoring of the D-type. The other possible anchoring modes are E- and F-type attached via two of its four carboxylic groups coming from two different bipyridine ligands. The carboxylic group either bridges two adjacent rows of titanium ions through bidentate coordination or interact with surface hydroxyl groups through hydrogen bonds. The remaining two carboxylic groups stay in a protonated state. According to their studies the bonding geometry of the E- and the F-type are thermodynamically most favorable. The ATR-FTIR data of the N3, N719, and N712 discussed below are consistent with F-type anchoring mode where the sensitizer adsorbs on the surface using two carboxylic groups.

The ATR-FTIR spectra of the N3, N719, and N712 complexes measured as a solid and in the adsorbed form onto TiO_2 films are shown in Figures 4 and 5, respectively. The N3 solid sample shows a strong broad band at 1720 cm^{-1} due to carboxylic acid groups (Figure 4a). It is interesting to note the presence of only one band in the carboxylic acid position compared to the PAS IR spectra where two bands were observed due to cis and trans carboxylic acid groups. However, the bandwidth of the carboxylic acid groups in ATR spectra (60 cm^{-1}) is larger than the difference between the cis and the trans carboxylic groups (40 cm^{-1}). The intense peak at 1229 cm^{-1} is assigned to υ(C−O) stretch.

The N719 complex that contains two carboxylic acid and two carboxylate groups shows bands at 1712 and 1608 cm^{-1} due to $\upsilon(-C{=}O)$ and $\upsilon(-COO^-as)$, respectively. The symmetric stretch of carboxylate group was observed at 1365 cm^{-1}. The intense peak at 1226 cm^{-1} is assigned to υ(C−O) stretch (Figure 4b). The FTIR spectra of the N712 complex show bands due

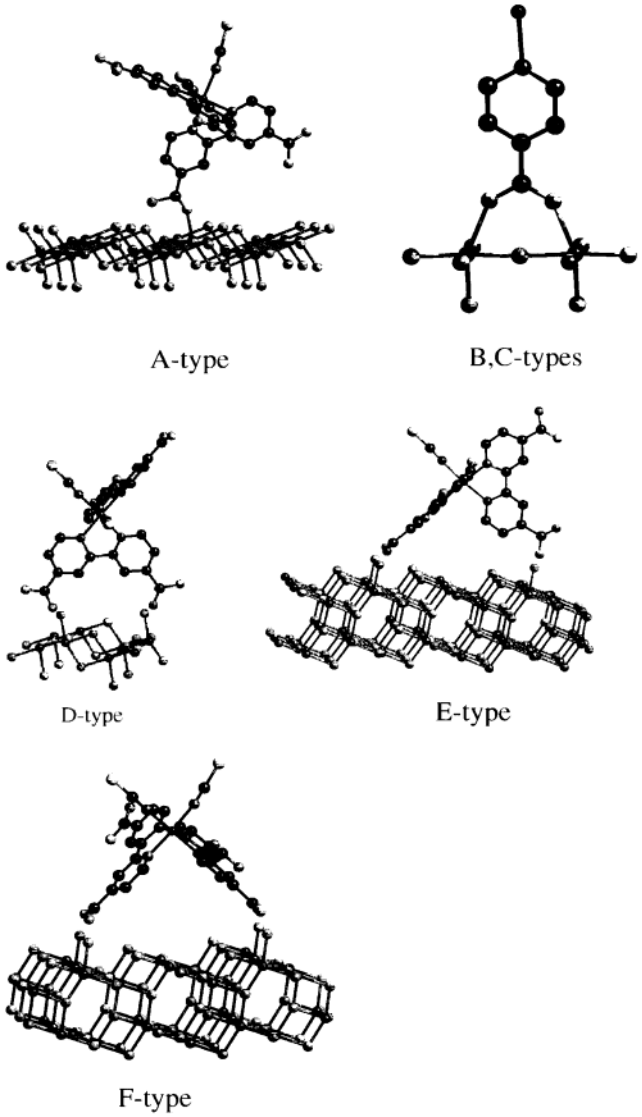

Figure 3. Possible anchoring modes for N3 sensitizer using carboxylic acid functional groups.

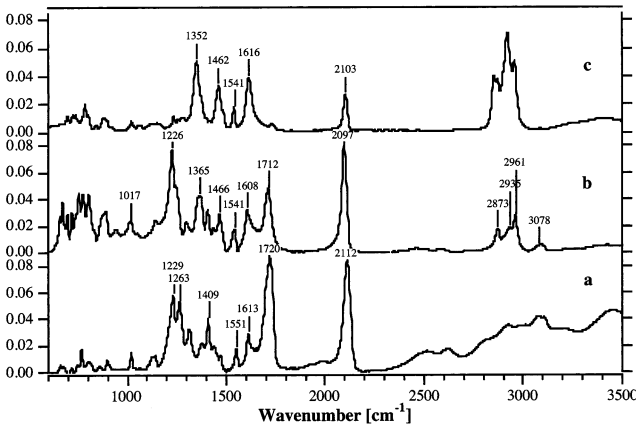

Figure 4. ATR-FTIR spectra of N3 (a), N719 (b), and N712 (c) obtained using solid samples.

to carboxylate groups asymmetric and symmetric at 1616 cm^{-1} ($-COO^-_{as}$) and 1352 cm^{-1} ($-COO^-_s$), respectively (Figure 4c).[26] The significant difference between the PAS mode and the ATR mode is the bandwidth, which is smaller and sharper (30 cm^{-1}) in the former case compared to that of the ATR mode. The band due to υ(NC) of the thiocyanate ligand was observed

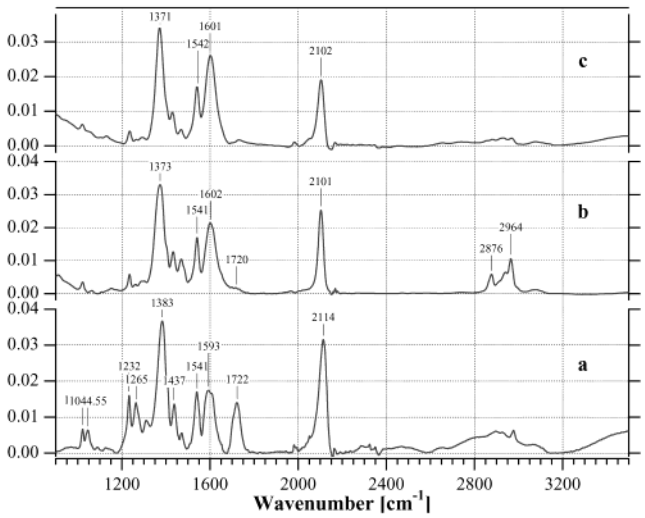

Figure 5. ATR-FTIR spectra of the TiO_2 films adsorbed by N3 (a), N719 (b), and N712 (c) dyes.

at 2112, 2097, and 2103 cm^{-1} in N3, N719, and N712 complexes, respectively. It is interesting to compare the intensity of the NCS peak in the N3, N719, and N712 complexes where in the later case it is lower than the former two complexes, which is due to differences in the dipole moment. The protons in both the complexes N3 and N719 are located trans to the NCS groups, which induces a larger dipole compared to the NCS groups in N712.

Figure 5a shows the ATR-FTIR spectrum of N3 adsorbed on TiO_2. The major difference between the solid and the adsorbed N3 spectra is the presence of carboxylate asymmetric 1593 cm^{-1} $\upsilon(-COO^-_{as})$ and symmetric 1383 cm^{-1} $\upsilon(-COO^-_s)$ bands together with carboxylic acid group at 1722 cm^{-1}. The presence of carboxylic acid and carboxylate groups in the IR spectra of adsorbed N3 on TiO_2 testifies that all the carboxylic acid groups are not dissociated or involved in the adsorption on the TiO_2 surface. On the other hand, complex N712 (Figure 5c) shows the presence of only carboxylate groups at 1601 $\upsilon(-COO^-_{as})$ and 1371 cm^{-1} $\upsilon(-COO^-_s)$, confirming the absence of ester bond between the complex and the TiO_2.

In the N3 and the N712, there are four anchoring groups. Because of steric reasons, anchoring of these complexes onto the TiO_2 surface using all the groups is not possible. However, the question arises as to how many groups are adsorbed on the surface and what is the anchoring mode? A comparison of the normalized intensities of the carboxylate group in the free and the adsorbed dyes with the bpy band at 1544 cm^{-1} indicate two carboxylate groups are involved in the anchoring of the dye onto the TiO_2 surface.

A carboxylate group can coordinate to the TiO_2 surface in number of ways: as a unidentate mode, as a chelating mode, and as a bridging bidentate mode (shown in Chart 2). The unidentate coordination of the carboxylate group removes the equivalence of the two oxygen atoms resulting to an ester type of bond formation between the carboxylic acid group and the TiO_2 surface. On the basis of the IR data of adsorbed N712 complex, this type of coordination can be ruled out, leaving only two possiblities, chelation and/or bridging coordination. However, for identifying the carboxylate-anchoring mode, on the basis of metal acetate complexes, several groups have used the difference between the asymmetric and symmetric bands in the free and the adsorbed state as criteria. Where, if the difference between the carboxylate group asymmetric and symmetric bands in the adsorbed state is lower than that in the

CHART 2

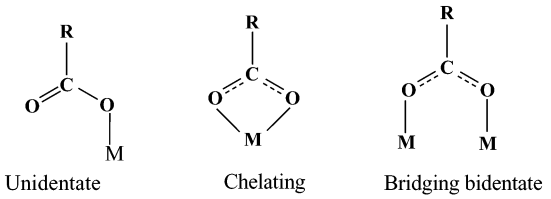

free state, then the anchoring mode is either bidentate chelation or bridging. If the difference is greater or equal to that in the free state, then anchoring mode is unidentate.[37]

The separation between the carboxylate group asymmetric and symmetric bands of N712 in the free (264 cm^{-1}) and the adsorbed state (230 cm^{-1}) suggest that this dye anchors either as bidentate chelation or as bridging coordination to the TiO_2.[38] The separation in the N3 and the N719 complexes between the carboxylate group asymmetric and symmetric bands in the adsorbed state is 211 and 227 cm^{-1}, consistent with bidentate chelation or bridging coordination mode. However, recent theoretical studies on the interaction of formic acid and sodium formate on anatase (101) surface showed that the formation of the bidentate chelation mode is highly unstable, leaving the possibility of bridging coordination mode.[39] Anchoring of the dye onto the TiO_2 surface using the bidentate chelation mode of the carboxylate group should result in enhanced stability for the sensitizer compared to the unidentate adsorption. Our findings are in excellent agreement with photoelectron spectroscopic data of N3 adsorption on TiO_2.[40]

The ATR-FTIR data of the N3 and the N712 complexes show that these dyes anchor onto the TiO_2 surface using two of its four carboxylic acid groups as a bridging coordination mode. Nonetheless, out of four anchoring groups, which of the two, i.e., cis, trans, or mixed carboxylic acid groups, remained unsolved? The N719 complex contains two carboxylic groups, which are trans to the NCS ligands, and two carboxylate groups, which are trans to each other. When complex N719 is adsorbed on the surface, it could adsorb using the carboxylic or carboxylate or both carboxylic and carboxylate groups. The FTIR spectra show (Figure 5b) the presence of mainly carboxylate groups, demonstrating that the complex is being adsorbed on the surface using the two carboxylic groups, which are trans to the NCS ligands (F-type). However, the presence of a small band (around 5%) at the carboxylic position indicates that around 5% of the complex is being adsorbed on the surface, employing one carboxylic acid and one carboxylate group (E-type).

3.3. NMR Spectroscopy. Proton NMR spectral data of N3, N719, and N712 CD_3OD solution shows six peaks in the aromatic region due to two different dcbpy ring protons, in which two pyridine rings are trans to the NCS ligands and the remaining two are trans to each other. The resonance peaks in the aliphatic region for complexes N719 and N712 are due to tetrabutylammonium cations. The integrated ratio of the aliphatic to aromatic protons shows the presence of two and four tetrabutylammonium cations in N719 and N712 complexes, respectively. The aromatic protons in N712 and N719 are high-field shifted compared to the protons in the N3 complex. The proton NMR spectra of the N3 complex isolated at pH = 2.5 show small peaks at lower field, which are due to linkage isomers that are difficult to separate using either column or recrystallization methods. However, it is striking to note the absence of linkage isomers in N719, which was isolated at pH 3.5. The reason for precipitation of N719 complex at pH 3.5 is the presence of bulky and hydrophobic tetrabutylammonium cations.

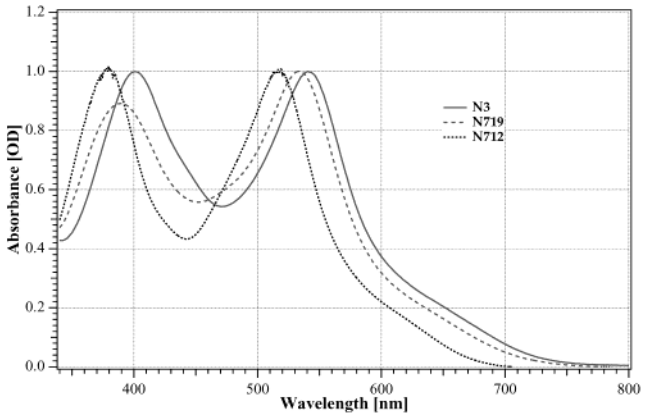

Figure 6. Absorption spectra of N3, N719, and N712 dyes in ethanol solution.

The proton decoupled carbon-13 NMR spectrum of the N3 complex in the aromatic region shows 13 clearly defined resonance peaks, which are 6 pairs and a single peak at 135 ppm. The 6 pairs are assigned to the pyridine carbons by comparing with known bipyridine complexes.[41] The single peak at 135 ppm is assigned to the carbon of the N-coordinated NCS ligand. Carbon-13 NMR shifts can be used to characterize the electron densities of the corresponding carbon. The downfield two resonances at 172.59 and 172.24 ppm in the N3 complex are assigned to the carboxylic acid carbons, which are slightly downfield shifted compared to those of N719 (168.25 and 168.03 ppm) and N712 (167.55 and 167.23 ppm), respectively. The high-field shift in the N712 complex reflects an increase in the electron density due to replacement of an electron withdrawing proton by tetrabutylammonium cations. Aliphatic carbons of tetrabutylammonium cations in N719 and N712 were observed at 54, 35, 16, and 9 ppm.

3.4. Absorption Spectra. Figure 6 shows a comparison of the absorption spectra of N3, N719, and N712 complexes in ethanol solution. The two broad visible bands at 538 and 398 nm in N3 are assigned to metal-to-ligand charge-transfer (MLCT) origin. The bands in the UV at 314 nm with a shoulder at 304 nm are assigned as intra ligand ($\pi-\pi^*$) charge-transfer transitions.[42] Deprotonation of the COOH groups blue shifts the $\pi-\pi^*$ charge-transfer band from 314 to 308 nm (not shown in the figure) and the low-energy MLCT band shifted to higher energy by 20 nm, from 538 to 518 nm. The blue shift is due to an increase in the energy of the LUMO of the ligand, causing the $\pi-\pi^*$ and d$\pi-\pi^*$ transitions to occur at higher energies. On the other hand, the low-energy MLCT band in N719 complex blue shift only by 3 nm (535 nm) compared to the N3 complex because the LUMO in N719 is already dictated by the presence of two protonated COOH groups similar to the N3.

The absorption spectra of the three complexes anchored on 7 μm thick TiO_2 nanocrystalline electrode were shown in Figure 7. The low-energy MLCT maximum in N712 is considerably red shifted upon adsorption onto the TiO_2 nanocrystalline electrode compared to the solution spectra. This is due to the fact that on the electrode the carboxylate groups bind to the TiO_2 surface in which Ti^{4+}acts as proton. The position of the low-energy MLCT band of N3 and N719 complexes in solution and anchored on TiO_2 nanocrystalline electrode is very similar because of the presence of protons in solution and Ti^{4+} in the adsorbed state. It is interesting to note that the rate of adsorption for N3 is much faster than that for N719, which in turn is faster than that for N712. For N712, dye adsorption on TiO_2 was very slow even if the dye concentration is 1 mM, due to its high

TABLE 1: Performance Characteristics of Photovoltaic Cells Based on Nanocrystalline TiO_2 Films Sensitized by N3 with Different Degrees of Protons

sensitizer	no. of protons	solvent for dye adsorption	current)mA/cm^2)	potential (mV)	fill factor	efficiency at 1.5 AM
N3	4	1:1 CH3CN + *tert*-BuOH	19 ± 0.5	600 ± 30	0.65 ± 0.05	7.4
N719	2	1:1 CH3CN + *tert*-BuOH	17 ± 0.5	730 ± 30	0.68 ± 0.05	8.4
N712	0	C2H5OH	13 ± 0.5	900 ± 30	0.7 ± 0.05	8.2
N3[TBA]3	1	5:95 CH3CN +*tert*-BuOH	16.8 ±0.5	770 ± 20	0.72 ± 0.05	9.3
N3[TBA]	3	1:1 CH3CN + *tert*-BuOH	17 ± 0.5	700 ± 20	0.65 ± 0.05	7.7

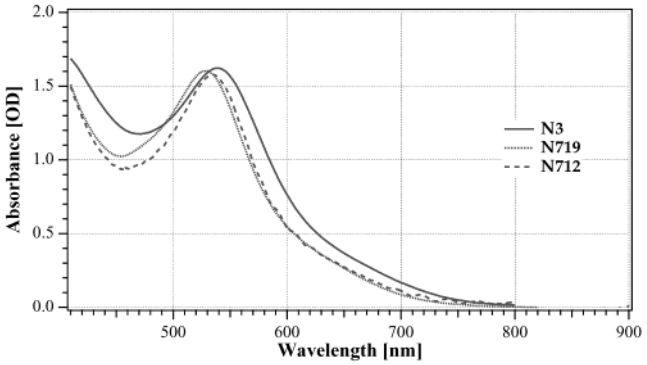

Figure 7. Absorption spectra of N3, N719, and N712 dyes adsorbed onto a nanocrystalline 7 μm thick TiO_2 films.

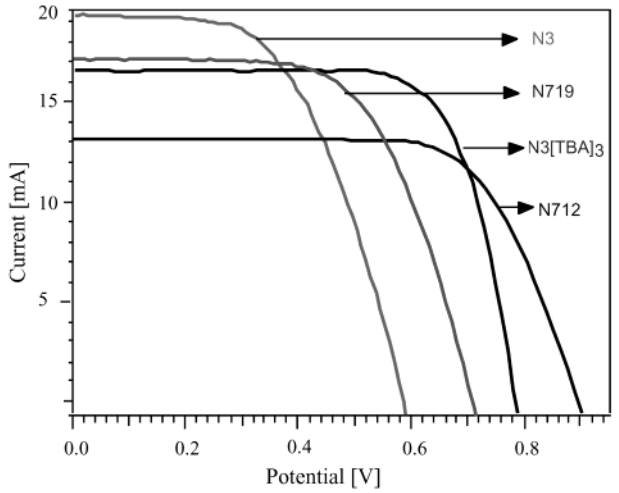

Figure 8. Photocurrent−voltage characteristics of nanocrystalline TiO_2 cell sensitized with N3 (contains 4 protons), N719 (contains 2 protons), N3[TBA]$_3$ (contains 1 proton), and N712 (contains zero proton) dyes measured under AM 1.5 sun using 1 cm^2 size of TiO_2 electrodes with I^-/I_3^- redox couple in methoxyacetonitrile (N3 = $[Ru(dcbpyH_2)_2(NCS)_2]$, N719 = $(Bu_4N)_2[Ru(dcbpyH)_2(NCS)_2]$, N3[TBA]$_3$ = $(Bu_4N)_3[Ru(dcbpyH)(dcbpy)(NCS)_2]$, and N712 = $(Bu_4N)_4[Ru(dcbpy)_2(NCS)_2]$).

solubility in organic solvents, which displaces the equilibrium between adsorption and desorption. Nonetheless, the dye loading increased significantly by increasing the dye concentration 100 times that shifts the equilibrium.

3.5. Photovoltaic Performance. The performance of N3 sensitizer and its various protonated forms on nanocrystalline TiO_2 electrodes have been studied, and the data are collected in Table 1. Figure 8 shows the current−voltage characteristics obtained with a sandwich cell under illumination by simulated AM 1.5 solar light. The photocurrent action spectra of these sensitizers show broad features covering a large part of the visible spectrum. The incident monochromatic photon-to-current conversion efficiency (IPCE) is plotted as a function of excitation wavelength and shows a plateau region at 85% for N3 complex whereas for N712 complex it is only about 70%. In the red region, the difference is even more pronounced. Thus, at 700 nm the IPCE value is twice as high for the N3 complex as compared to the N712 complex. Consequently, the short circuit photocurrent is 19 ± 1 mA/cm^2 for the N3 complex, whereas it is only about 13 ± 1 mA/cm^2 for the N712 complex. However, it is impressive that the photovoltage for N712 is 900 mV, which is 300 mV higher than that for N3. The increased open circuit potential in the former case is the result of negative shift of the Fermi level that increases the gap between the redox couple iodide/triiodide and the Fermi level. The photovoltaic performance of N719 that carries two protons shows 17 ± 1 mA current and 730 mV potential. The fill factor also increases with increasing open circuit potential of the dye-sensitized solar cell. The data presented in Table 1 suggest that the one proton dye is the optimum for high-power conversion efficiency of the cell.

The decrease in the IPCE of N712 compared to that of N3 is due to the influence of protons on the energetics of the TiO_2 conduction band and therefore on the energetics of electron injection. The second possible reason could be slow regeneration of the dye by the redox couple because of the decreased driving force between the dye and the redox couple. Recently, Tachibana et al. reported electron injection kinetics for nanocrystalline TiO_2 electrodes sensitized with the N3 and the N719 dyes.[43] In their studies, they found that the electron injection kinetics for N719 is retarded 30-fold compared to that for N3. Their data imply that the low IPCE in the N712 complex compared to the N3 dye is due to the energetics of the TiO_2 conduction band rather than the decrease in the driving force between the sensitizer and the redox couple.

4. Conclusions

On the basis of the FTIR data, we have made a quantitative analysis of the adsorption mode of sensitizers N3, N719, and N712 on a TiO_2 surface. The data show that these dyes anchor onto the TiO_2 surface using two of their four carboxylic acid groups in a bridging coordination consistent with F-type anchoring mode. The performances of N3 sensitizer with different degrees of protonation were investigated in nanocrystalline TiO_2 based solar cells. We have shown the important effect exerted by the proton content of the complex on both the short circuit photocurrent and open circuit photovoltage of dye-sensitized nanocrystalline solar cell. The monoprotonated form of the N3 dye gave 16.8 mA/cm^2 current, 0.77 V open circuit potential, and 0.72 fill factor, yielding total power conversion efficiency of 9.3 under AM 1.5 sunlight.

Acknowledgment. We acknowledge financial support of this work by the Swiss Science Foundation, Swiss Federal Office for Energy (OFEN), U.S. Air Force Research Office under contract number F61775-00-C0003, and the Institute for Applied Photovoltaics (INAP, Gelsenkirchen, Germany).

References and Notes

(1) McConnell, R. D. *Renewable Sustainable Energy Rev.* **2002**, *6*, 273.

(2) Asbury, J. B.; Ellingson, R. J.; Ghosh, H. N.; Ferrere, S.; Nozik, A. J.; Lian, T. *J. Phys. Chem. B* **1999**, *103*, 3110.
(3) Ellingson, R. J.; Asbury, J. B.; Ferrere, S.; Ghosh, H. N.; Sprague, J. R.; Lian, T.; Nozik, A. J. *J. Phys. Chem. B* **1998**, *102*, 6455.
(4) van de Lagemaat, J.; Frank, A. J. *J. Phys. Chem. B* **2001**, *105*, 11194.
(5) Hara, K.; Horiuchi, H.; Katoh, R.; Singh, L. P.; Sugihara, H.; Sayama, K.; Murata, S.; Tachiya, M.; Arakawa, H. *J. Phys. Chem. B* **2002**, *106*, 374.
(6) Islam, A.; Sugihara, H.; Singh, L. K.; K., H.; Katoh, R.; Nagawa, Y.; Yanagida, M.; Takahashi, Y.; Murata, S.; Arakawa, H. *Inorg. Chim. Acta* **2001**, *322*, 7.
(7) Kubo, W.; Kitamura, T.; Hanabusa, K.; Wada, Y.; Yanagida, S. *Chem. Commun.* **2002**, 374.
(8) Boschloo, G.; Lindstrom, H.; Magnusson, E.; Holmberg, A.; Hagfeldt, A. *Photochem. Photobiol., A: Chem.* **2002**, *148*, 11.
(9) Hagfeldt, A.; Grätzel, M. *Acc. Chem. Res.* **2000**, *33*, 269.
(10) Ferrere, S.; Gregg, B. A. *J. Phys. Chem. B* **2001**, *105*, 7602.
(11) Heimer, T. A.; Heilweil, J.; Bignozzi, C. A.; Meyer, G. J. *J. Phys. Chem. A* **2000**, *104*, 4256.
(12) Nogueira, A. F.; Durrant, J. R.; De Paoli, M.-A. *Adv. Mater.* **2001**, *13*, 826.
(13) Oskam, G.; Bergeron, B. V.; Meyer, G. J.; Searson, P. C. *J. Phys. Chem. B* **2001**, *105*, 6867.
(14) Sauvé, G.; Cass, M. E.; Doig, S. J.; Lauermann, I.; Pomykal, K.; Lewis, N. S. *J. Phys. Chem.* **2000**, *104*, 3488.
(15) De Paoli, M.-A.; Machado, D. A.; Nogueira, A. F.; Longo, C. *Electrochim. Acta* **2001**, *46*, 4243.
(16) Hou, Y.-J.; Xie, P.-H.; ZJing, B.-W.; Cao, Y.; Xiao, X.-R.; Wang, W.-B. *Inorg. Chem.* **1999**, *38*, 6320.
(17) Kumara, G. R. A.; Konno, A.; Shiratsuchi, K.; Tsukahara, J.; Tennakone, K. *Chem. Mater.* **2002**, *14*, 954.
(18) Lemon, B.; Hupp, J. T. *J. Phys. Chem. B.* **1999**, *103*, 3797.
(19) Lees, A. C.; Kleverlaan, C. J.; Bignozzi, C. A.; Vos, J. G. *Inorg. Chem.* **2001**, *40*, 5343.
(20) Xie, P.-H.; Hou, Y. J.; Zhang, B. W.; Cao, Y.; Wu, F.; Tian, W.-J.; Shen, J. C. *J. Chem. Soc., Dalton Trans.* **1999**, 4217.
(21) Nazeeruddin, M. K.; Zakeeruddin, S. M.; Humphry-Baker, R.; Kaden, T. A.; Grätzel, M. *Inorg. Chem* **2000**, *39*, 4542.
(22) Rice, C. R.; Ward, M. D.; Nazeeruddin, M. K.; Grätzel, M. *New J. Chem.* **2000**, *24*, 651.
(23) Yan, S. G.; Hupp, J. T. *J. Phys. Chem.* **1996**, *100*, 6867.
(24) Pelet, S.; Moser, J. E.; Graetzel, M. *J. Phys. Chem. B* **2000**, *104*, 1791.
(25) Cahen, D.; Hodes, G.; Grätzel, M.; Guilemoles, J. F.; Riess, I. *J. Phys. Chem. B* **2000**, *104*, 2053.
(26) Nazeeruddin, M. K.; Amirnasr, M.; Comte, P.; Mackay, J. R.; McQuillan, A. J.; Grätzel, M. *Langmuir* **2000**, *16*, 8525.
(27) Nazeeruddin, M. K.; Zakeeruddin, S. M.; Humphry-Baker, R.; Jirousek, M.; Liska, P.; Vlachopoulos, N.; Shklover, V.; Fischer, C. H.; Grätzel, M. *Inorg. Chem.* **1999**, *38*, 6298.
(28) Nazeeruddin, M. K.; Kay, A.; Rodicio, I.; Humphry-Baker, R.; Muller, E.; Liska, P.; Vlachopoulos, N.; Grätzel, M. *J. Am. Chem. Soc.* **1993**, *115*, 6382.
(29) Finnie, K. S.; Bartlett, J. R.; Woolfrey, J. L. *Langmuirr* **1998**, *14*, 2744.
(30) Fillinger, A.; Parkinson, B. A. *J. Electrochem. Soc.* **1999**, *146*, 4559.
(31) Shklover, V.; Ovehinnikov, Y. E.; Braginsky, L. S.; Zakeeruddin, S. M.; Grätzel, M. *Chem. Mater.* **1998**, *10*, 2533.
(32) Asbury, J. B.; Hao, E.; Wang, Y.; Ghosh, H. N.; Lian, T. *J. Phys. Chem. B* **2001**, *105*, 4545.
(33) Hannappel, T.; Burfeindt, B.; Storck, W.; Willig, F. *J. Phys. Chem. B* **1997**, *101*, 6799.
(34) Eskelinen, E.; Luukkanen, S.; Haukka, M.; Ahlgrén, M.; Pakkanen, T. A. *J. Chem. Soc., Dalton Trans.* **2000**, 2745−2752.
(35) Wolfbauer, G.; Bond, A. M.; Eklund, J. C.; MacFarlane, D. R. *Solar Energy Mater. Solar Cells* **2001**, *70*.
(36) Murakoshi, K.; Kano, G.; Wada, Y.; Yanagida, S.; Miyazaki, H.; Matsumoto, M.; Murasawa, S. *J. Electroanal. Chem.* **1995**, *396*, 27.
(37) Deacon, G. B.; Phillips, R. J. *Coord. Chem. Rev.* **1980**, *33*, 227.
(38) Nakamoto, K. *Infrared and Raman Spectra*, 4th ed.; John Wiley & Sons: New York, 1986.
(39) Vittadini, A.; Selloni, A.; Rotzinger, F. P.; Graetzel, M. *J. Phys. Chem. B* **2000**, *104*, 1300.
(40) Westermark, K.; Rensmo, H.; Siegbahn, H.; Keis, K.; Hagfeldt, A. *J. Phys. Chem. B* **2002**, *106*, 10102.
(41) Cook, M. J.; Lewis, A. P.; McAuliffe, G. S. G. *Org. Magn. Reson.* **1984**, *22*, 388.
(42) Root, M. J.; Sullivan, B. P.; Meyer, T. J.; Deutsch, E. *Inorg. Chem.* **1985**, *24*, 2731.
(43) Tachibana, Y.; Nazeeruddin, M. K.; Graetzel, M.; Klug, D. R.; Durrant, J. R. *Chem. Phys.* **2002**, *284*, 127.